Journal of Materials Chemistry A

Accepted Manuscript

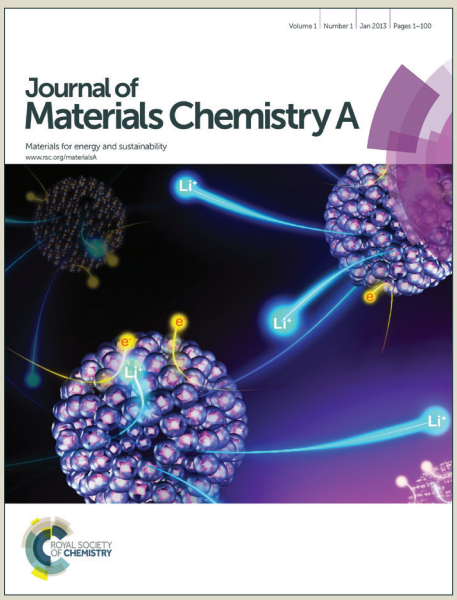

ROYAL SOCIETY OF CHEMISTRY

www.rsc.org/materialsA

ARTICLE TYPE www.rsc.org/xxxxxx | XXXXXXXX

Graphitic carbon nitride nanosheets coated carbon black as high-performance PtRu catalyst support material for methanol electrooxidation

Cun-Zhi Li,[ab] Zhen-Bo Wang,*[a] Xu-Lei Sui,[a] Li-Mei Zhang,[a] Da-Ming Gu[b] and Shuo Gu[c]

Received (in XXX, XXX) Xth XXXXXXXXX 200X, Accepted Xth XXXXXXXXX 200X
First published on the web Xth XXXXXXXXX 200X
DOI: 10.1039/b000000x

PtRu supported on C@g-C_3N_4 NS (g-C_3N_4 nanosheets coated Vulcan XC-72 carbon black) catalyst has been prepared by microwave-assisted polyol process (MAPP). The results of electrochemical measurements show that the PtRu/C@g-C_3N_4 NS catalyst has excellent activity due to more uniform dispersion and smaller size of PtRu nanoparticles (PtRu NPs), and higher stability ascribed to the stronger metal–support interaction (SMSI) between PtRu NPs and composite support. The physical characteristics such as X-ray diffraction (XRD), transmission electron microscopy (TEM) and X-ray photoelectron spectroscopy (XPS) have indicated that bulk g-C_3N_4 shell outside of the as-prepared C@bulk g-C_3N_4 (bulk g-C_3N_4 coated Vulcan XC-72 carbon black, C@bulk g-C_3N_4) indeed exfoliated to layered g-C_3N_4 nanosheets and formed a composite material of Vulcan XC-72 coated with g-C_3N_4 nanosheets. Furthermore, the results present the mass catalytic activity of PtRu/C@g-C_3N_4 NS catalyst substantially enhanced, which is a factor of 2.1 times higher than that of the PtRu/C catalyst prepared by the same procedure and the accelerated potential cycling tests (APCT) show that the PtRu/C@g-C_3N_4 NS catalyst possesses 14% higher stability and much greater poison tolerance than as-prepared PtRu/C. The significantly enhanced performance for PtRu/C@g-C_3N_4 NS catalyst is ascribed to the reasons as follows: the inherently excellent mechanical resistance and stability of g-C_3N_4 nanosheets in acidic and oxidative environments; the increased electron conductivity of support by forming a core-shell structure of C@g-C_3N_4 NS; SMSI between metal NPs and composite support. Based on this novel approach to C@g-C_3N_4 NS hybrid nanostructure, many other interesting applications might also be discovered.

1. Introduction

Platinum and ruthenium bimetallic catalyst (PtRu) based on the bifunctional mechanism is considered to be the most efficient anodic catalyst for methanol electrooxidation in direct methanol fuel cells (DMFCs).[1-8] However, because of the limited resources and high cost of platinum or ruthenium, the utilization efficiency of the noble metal must be improved.[3, 9] An efficient way is to disperse them onto a suitable support.[10-18] Currently, the most widely used support is carbon black Vulcan XC-72R, which has high surface area and excellent electrical conductivity.[19, 20] Nevertheless, Pt nanoparticles (NPs) can get "buried" inside the pores and leading the reduction of the active triple-phase boundary accessible for electrochemical reaction.[21] Furthermore, Vulcan XC-72R is electrochemically unstable at high potentials, leading to corrosion after extended operation in acidic media and varying potentials.[22]

Graphitic carbon nitride (g-C_3N_4) polymer has been demonstrated as a kind of advanced support material for Pt and Pt- based NPs due to its much lower price and excellent mechanical resistance and anticorrosion ability in acidic and oxidative environments,[23-25] as well as the abundant Lewis acid and base sites (terminal and bridging NH− groups and lone pairs of N in triazine/heptazine rings, respectively) that are potential anchoring sites for Pt[26] and adsorption sites for CO.[27, 28] Therefore, to explore the possibility of employing g-C_3N_4 as PtRu catalyst supporting material for DMFC is very necessary and meaningful.

However, due to the non-conductive nature and the low surface areas of bulk g-C_3N_4 prepared by conventional thermal polymerization, it necessarily deserves the investigation of the structural design of catalysts to weaken the side-effects resulting from the low electron conductivity and the low surface areas.[29] Up to now, many researchers have investigated the g-C_3N_4 as metal free catalysts for oxygen reduction reaction,[30-32] but rare papers have focused on the structural design of a supporting material for PtRu anode catalysts in DMFCs. Mansor and co-workers[27] have prepared three different graphitic carbon nitride materials as catalyst support materials for PEMFCs, which supported Pt electrocatalysts have higher methanol oxidation activity per ECSA, compared to Pt/Vulcan. However, the conductivity of those catalysts is much lower than that of the commercial Pt/Vulcan. Kim and co-workers[33] demonstrated the synthesis of well-ordered nanoporous graphitic carbon nitride by polymerization of cyanamide using colloidal silica as a template at 550 °C, which was proved to be promising as a catalyst support in DMFCs, but

[a] *School of Chemical Engineering and Technology, Harbin Institute of Technology, No.92 West-Da Zhi Street, Harbin, 150001 China. E-mail: wangzhb@hit.edu.cn; Tel.: +86-451-86417853; Fax: +86-451-86418616*
[b] *School of Science, Harbin Institute of Technology, No.92 West-Da Zhi Street, Harbin, 150001 China*
[c] *Department of Electrical and Computer Engineering, The George Washington University, Washington, DC, 20052, USA*

† Electronic supplementary information (ESI) available. See DOI: 10.1039/b000000x

the process required multiple steps including the preparation and the removal of template.

In this work, we firstly prepared graphitic carbon nitride nanosheets coated Vulcan XC-72R carbon (C@g-C_3N_4 NS) supporting material using a convenient method and then deposit the PtRu NPs using a fast and facile microwave assisted polyol process (MAPP).[34] The overall procedure does not require complicated steps. The results show that the C@g-C_3N_4 NS composite support PtRu (PtRu/C@g-C_3N_4 NS) catalyst exhibits a significantly higher catalytic activity and stability, while the disadvantages from the poor electron conductivity and the low surface areas of bulk g-C_3N_4 are nearly nonexistent.

2. Experimental

2.1. Materials preparation

2.1.1 Preparation of C@bulk g-C_3N_4 precursor. The bulk g-C_3N_4 coated Vulcan XC-72 carbon black (C@bulk g-C_3N_4) precursor material was accomplished as follows. Firstly, 200mg Vulcan XC-72R and 4.0g $CO(NH_2)_2$ was dispersed into 20 mL H_2O (Millipore, 18.25 MΩ·cm) in 50 mL beaker under ultrasonic treatment for 1 hour to form uniform ink. And then the ink was dried at 70°C in an alumina boat and heated in the tube furnace under argon. The temperature was raised to 550°C at 10°C min^{-1} for 2 h. The product was cooled to room temperature in argon and then ground to uniform.

2.1.2 Preparation of C@g-C_3N_4 NS support. The C@g-C_3N_4 NS composite support was prepared from C@bulk g-C_3N_4 precursor. A finely ground C@bulk g-C_3N_4 was thermal decompositionre in an alumina boat into a quartz tube in a tubular furnace under nitrogen flow at 600°C for 2h by a heating rate of 10°C min^{-1}. And then product was cooled to room temperature in argon.

2.1.3 Preparation of PtRu/C@g-C_3N_4 NS and PtRu/C. Hexachloroplatinic acid ($H_2PtCl_6·6H_2O$) and ruthenium chloride ($RuCl_3$) were purchased from Beijing, China. Vulcan XC-72 carbon black with mean particle size of 20 nm was purchased from Cabot and 5 wt.% Nafion solution was obtained from Dupont. Except where specified, all chemicals were of analytical grade and used as received. The deposition of PtRu NPs on a C@g-C_3N_4 NS supports were prepared using a microwave-assisted polyol process [34-36] and the atomic ratio of Pt/Ru was adjusted to that of the commercial catalyst (atomic ratio of 1:1). Briefly, a calculated amount of C@g-C_3N_4 NS was dispersed into mixture of ethylene glycol and isopropyl alcohol under ultrasonic treatment for 1 h. After the suspension was stirred for 3 h, a selected amount of H_2PtCl_6-EG and $RuCl_3$-EG solution was added into the uniform carbon ink drop by drop with urgent agitation for 3 h. Followed by adjusting the pH (pHS-32 meter) to 8 by using a 1 mol L^{-1} NaOH ethylene alcohol solution, the suspension was subjected to consecutive microwave heating for 50 s in a microwave oven (from Galanz Ltd., 800 W) under flowing Ar. After the solution was cooled to room temperature, pH was adjusted to 2 by HNO_3 aqueous solution, which was then stirred for 12 h. Finally, the product was filtered, washed for several times with ultrapure water (Millipore, 18.2 MΩ·cm). The obtained PtRu/C@g-C_3N_4 NS catalysts were dried for 3 h at 80°C and then were stored in a vacuum vessel.

2.1.4 Preparation of working electrode. The catalyst ink was prepared by ultrasonically dispersing catalyst powders in an appropriate amount of ultrapure water. The glassy carbon (GC) working electrode with 3 mm of diameter was polished with 0.05 mm alumina suspensions to a mirror finish before each experiment and served as an underlying substrate of the working electrode. The catalyst ink of 5 μL was dropped onto a glassy carbon working electrode, and was dried for 15 min. Later, 5 μL of Nafion solution (5 wt. % solution in a mixture of lower aliphatic alcohols and DuPont water) was spread on the surface of electrode, and dried in air. In all cases, the total loading of metal was 28 μg cm^{-2}.

2.2 Electrochemical measurements

Electrochemical measurements were performed by using a CHI 650D potentiostat and a conventional three-electrode electrochemical cell. The counter electrode was Pt sheet of 1 cm^2 plate and Hg/Hg_2SO_4 electrode (–0.68 V relative to reversible hydrogen electrode, RHE) was used as the reference electrode. The PtRu/C@g-C_3N_4 NS and as-prepared PtRu/C catalysts electrodes were used as the working electrode. The electrochemical measurements of the catalysts were carried out in a glass sealed cell containing 0.5 mol L^{-1} H_2SO_4 and 0.5 mol L^{-1} CH_3OH solutions at 25 ± 1°C. Highly purified argon gas was purged into the solution for 20 min to eliminate oxygen. Due to a slight interference from the Nafion film, the working electrode was electrochemically cleaned by continuous cycling at 50 mV s^{-1} until a stable response was obtained before the measurement curves were recorded.

The stability of the catalyst was evaluated by the accelerated potential cycling test (APCT) which was conducted within the potential range of 0.05–1.20 V (versus RHE) with a scanning rate of 50 mV s^{-1}. All potentials are reported with respect to reversible hydrogen electrode in this paper.

The electroactive specific surface area of catalyst was determined by CO_{ad} stripping voltammetry, assuming the formation of a monolayer of linearly adsorbed CO and the coulombic charge required for oxidation of CO_{ad} to be 420 mC cm^{-2}. The voltammetry was carried out in 0.5 mol L^{-1} H_2SO_4 at 25°C with a scanning rate of 50 mV s^{-1}.

Electrochemical impedance spectroscopy (EIS) was obtained at frequencies between 100 kHz and 0.01 Hz with 12 points per decade. The amplitude of the sinusoidal potential signal was 5 mV.

2.3 Characterizations of physical properties

2.3.1 X-ray diffraction (XRD). The D/max-RB diffractometer (made in Japan) using a Cu Ka X-ray source operating at 45 kV and 100 mA, scanning at a rate of 4º min^{-1} with an angular resolution of 0.05º was used to obtain the XRD patterns of all catalysts.

2.3.2 Transmission electron microscopy (TEM). TEM images of all samples were characterized by using a TECNAI G2 F30 field emission transmission electron microscope with a spatial resolution of 0.17 nm. Before taking the electron micrographs, the samples were prepared by ultrasonically dispersing the catalyst powder in ethanol. A drop of the suspension was deposited on a standard copper grid coated with carbon film. The copper grid was then dried overnight. The applied voltage was 300 kV.

2.3.3 X-ray photoelectron spectroscopy (XPS). To determine the surface properties of the catalysts, XPS analysis was carried out by using the Physical Electronics PHI model 5700 instrument. Before XPS analysis, all samples were dried in vacuum at 80 °C overnight. The take-off angle of the sample to analyzer was 45° and the Al X-ray source was operated at 250 W. Survey spectra were collected at a pass energy (PE) of 187.85 eV over a binding energy range from 0 eV to 1300 eV. High binding energy resolution multiplex data for the individual elements were collected at a PE of 29.55 eV. During all XPS experiments, the pressure inside the vacuum system was maintained at 1×10^{-9} Pa.

2.3.4. Fourier transform infrared (FT-IR) spectra. FT-IR spectra of the C@g-C_3N_4 was recorded on Nicolet Magna 550 FT-IR spectrometer. The samples for FT-IR studies were prepared by suspending approximately 6 mg of composite support in 15 ml isopropyl alcohol by sonication for several minutes. One drop of this solution was sprayed onto silicon wafer and a uniform thin film on the IR transparent silicon substrate was thus obtained. FT-IR studies were carried out in the range of 400–4000 cm^{-1} in the absorbance mode.

3. Results and discussion

Scheme 1 shows the four principal steps for preparation of the PtRu/C@g-C_3N_4 NS catalyst as follows: (1) the mixing of Vulcan XC-72R carbon black and urea, (2) the preparation of C@bulk g-C_3N_4 precursor by thermal polymerizing of urea, (3) the exfoliating of bulk g-C_3N_4 shell to form g-C_3N_4 nanosheets at the decomposition temperature of g-C_3N_4 and finally (4) the deposition of PtRu NPs onto the C@g-C_3N_4 NS support. Although carbon nitride has been demonstrated as a promising support material due to its excellent mechanical resistance and anticorrosion ability in acidic and oxidative environments comparing with the carbon black, its non-conductive nature and

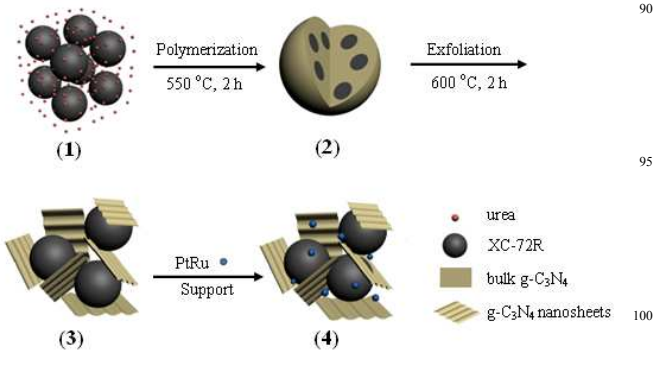

Scheme 1 Schematic illustration of the PtRu/C@g-C_3N_4 NS preparation process.

low surface areas still exist and impede its application in electrocatalyst field. For solving this problem, the C@bulk g-C_3N_4 precursor has been controllability exfoliated to C@g-C_3N_4 NS at the decomposition temperature of g-C_3N_4 about 600 °C. Through this method, the Vulcan XC-72R carbon black was uniformity coated with layered g-C_3N_4 nanosheets as shown in Scheme 1 (3). In addition, PtRu NPs were designed to deposit more on g-C_3N_4 nanosheets in Scheme 1 (4) due to the fact that the abundant Lewis acid and base sites of g-C_3N_4 augment deposition sites for PtRu NPs. The existence of g-C_3N_4 in C@g-C_3N_4 NS not only can improve its electrochemical stability at high potentials, but can enhance the interaction between PtRu NPs and support materials.

The greatly increased volume (see Fig. S1 in ESI for details†) of C@g-C_3N_4 NS composite sample indicates the bulk g-C_3N_4 shell is exfoliated to layered g-C_3N_4 nanosheets at the decomposition temperature of g-C_3N_4, which have larger surface areas than bulk g-C_3N_4.[25] The chemical structures of the samples were further analyzed by FTIR and the results were shown in Fig. 1. The board

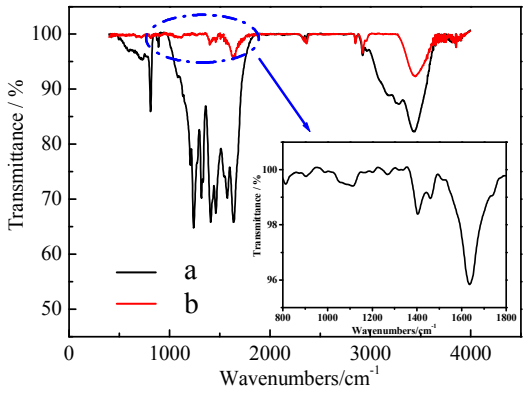

Fig. 1 FTIR spectrum of the C@bulk g-C_3N_4 (a) and C@ g-C_3N_4 NS (b).

peaks between 3000 and 3500 cm^{-1} corresponded to the N–H band.[37] The peaks at 1251, 1325, 1419, 1571, and 1639 cm^{-1} were contributed to the typical stretching modes of CN heterocycles. In addition, the characteristic breathing mode of triazine units at 810 cm^{-1} is observed.[31] Compared with the strong characteristic peak of g-C_3N_4 between 1200 cm^{-1} and 1700 cm^{-1} for C@bulk g-C_3N_4,[38] which of the C@g-C_3N_4 NS is weak. This can be attributed to the thermal decomposition of bulk g-C_3N_4 shell after heating at 600 °C for 2h, which lead to the reduction of g-C_3N_4 content in sample.

XRD analysis was carried out to investigate the crystal structure of the samples. Fig. 2 shows the XRD patterns of the as-prepared PtRu/C and the PtRu/C@g-C_3N_4 NS catalysts. In each XRD pattern, besides the diffraction peak of C(002) at 24.7, 2θ values of

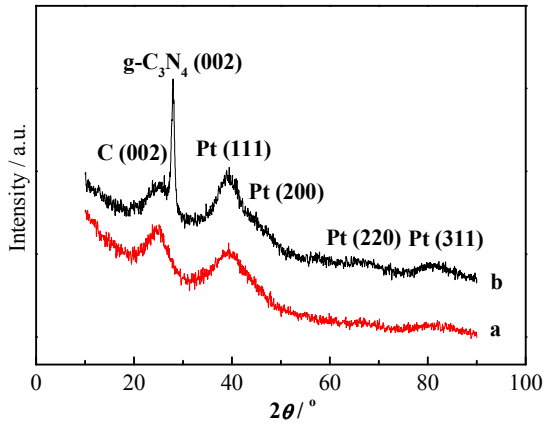

Fig. 2 XRD patterns of the PtRu/C catalyst (a) and the PtRu/C@g-C_3N_4 NS catalyst (b).

the other four peaks correspond to the (111), (200), (220), and (311) crystal planes of crystalline face-centered cubic Pt.[39] Therein, no recognisable diffractions of metallic Ru and/or Ru oxides are

consisted with our precious work.[40] As shown in Fig. 2, PtRu nanoparticles Pt (111) peak at 39.8° slightly shifted to higher 2θ which corresponds to a decrease in lattice constant compared to that of pure platinum at 39.6°, implying that the Ru may slightly enter Pt fcc lattice to form PtRu alloy.[41] And moreover, it is reasonable to confirm that the Ru mostly exists as amorphous metallic state Ru and an amount of hydrous ruthenium oxides in the catalyst, but they are not clearly detected by XRD. Guo et al.[42] also reported that some of Ru belongs to an amorphous phase in polyol-synthesised PtRu/C or commercial PtRu/C catalysts. In addition, the strong peak at ~ 27.5° for the PtRu/C@g-C_3N_4 NS corresponds to a repeat distance of ~ 0.32 nm that correlates with the (002) reflection usually observed for graphitic materials, which usually indicates the existence of g-C_3N_4.[43, 44]

Fig. 3 shows the TEM images of PtRu/C@g-C_3N_4 NS and as-prepared PtRu/C catalysts before and after accelerated potential cycling tests (APCT).[34] And the TEM image of the C@bulk g-C_3N_4 is shown in Fig. S2 (in ESI for details†). From Fig. S2, it can be clearly seen that the Vulcan XC-72R is totally encased in bulk g-C_3N_4 that consisting of layered solid agglomerates with a size of several micrometers. However, by heating at 600 ^oC for 2 h, the bulk g-C_3N_4 shell is exfoliated to g-C_3N_4 nanosheets about 38 nm estimated from Fig. 3A and Fig. 3B. Combining with the fact of Fig. S1, it can be concluded that the layered g-C_3N_4 nanosheets have been synthesized through a thermal exfoliation method. g-C_3N_4 nanosheets with a large surface area not only can improve its electron conductivity by decreasing the charge–transfer resistance,[37, 45] but benefit the deposition of PtRu NPs. Therefore, it can be obviously seen from Fig 3A and Fig. 3B that the PtRu NPs deposit on C@g-C_3N_4 NS surface more uniformly than as-prepared PtRu/C catalyst in Fig. 3C and Fig. 3D. With regard to the catalysts after APCT, the average sizes of PtRu NPs for PtRu/C@g-C_3N_4 NS and PtRu/C catalysts grow from initial 2.5 and 2.2 nm to 4.0 and 2.6 nm, increasing by 18% and 60%, respectively. Thus the extent of layered g-C_3N_4 effectively anchors the crystallites and inhibits migration and agglomeration (coalescence) of the PtRu NPs because of its abundant Lewis acid and base sites or the stronger metal–support interaction (SMSI).

XPS is an efficient method to analyze chemical state information of elements. The wide-scan XPS spectrum and the curves fitting of Pt 4f, Ru 3d, and N 1s peaks of the X-ray photoelectron spectra for PtRu/C@g-C_3N_4 NS and as-prepared PtRu/C catalysts are shown in Fig. 4. The curves fitting of Pt 4f, C 1s, and O 1s peaks of the X-ray photoelectron spectra for samples are in accordance with our previous work.[34] The surface elemental compositions of both catalysts are provided in Table 1. Compared with the surface atomic ratio of Pt/Ru for PtRu/C catalyst, that of the PtRu/C@g-C_3N_4 NS is more close to 1:1 leading a high-performance for methanol electrooxidation. This is possibly because of the strong interaction between nitrogen and metal atoms during the MAPP. Furthermore, the nitrogen atomic concentration of PtRu/C@g-C_3N_4 NS is about 15.22%. The N 1s peak (see from Fig. 4B) of PtRu/C@g-C_3N_4 NS consists of four components centred at 399.07, 400.14, 401.43 and 405.1 eV, which can be attributed to C≡N, C–N, –NH_2 and =NH, respectively. The results of the Pt 4f fitted peak positions and compositions obtained from the XPS analysis are summarized in Table 2. Not surprisingly, the Pt(0) peaks of PtRu/C@g-C_3N_4 NS shows a shift of the Pt 4f

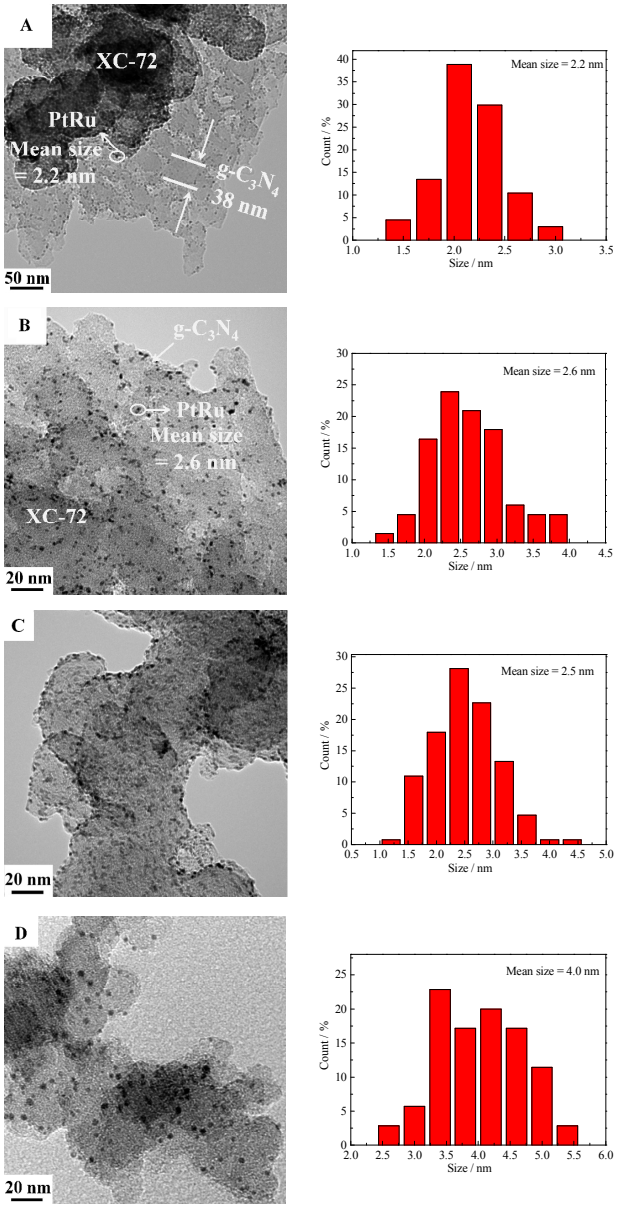

Fig. 3 TEM images and the size distributions of PtRu/C@g-C_3N_4 NS (A, B) and as-prepared PtRu/C (C, D) catalysts before (A, C) and after (B, D) APTC

binding energy to the direction of higher energies by about 0.19 eV in comparison with that of as-prepared PtRu/C catalyst, indicating further the SMSI between Pt nanoparticles and g-C_3N_4 support. This result is consistent with the results of previous studies of Pt/N-modified carbon catalysts systems due to the proposed occurrence of electron-donation from nitrogen defects to Pt in N-doped systems.[46] Moreover, the content of Pt(IV) decreases by 5.83%, demonstrating that PtRu/C@g-C_3N_4 NS has higher stability relative to as-prepared PtRu/C catalyst because of more corrosion resistance of Pt(0) and Pt(II) than that of Pt(IV).[47] As for the curve fitting results of Ru 3p in Table 3, ruthenium is largely present in its oxide forms, which is consisted with the result of XRD in Fig. 2. The presence of hydrous ruthenium oxide in the practical nanoscale Pt-Ru electrocatalysts offers more important

contributions to the electrocatalytic oxidation of methanol than Ru alloy.[48, 49] In addition, the Ru 3p peaks of PtRu/C@g-C_3N_4 NS catalyst shows a stronger shift of higher energies in comparison with that of the as-prepared PtRu/C, which correspond to Pt 4f fitting results.

Table 1 Fitting results of the XPS survey spectrum. Values are reported in % of the elements content.

Sample	C	N	O	Pt	Ru
PtRu/C	84.94	—	10.71	2.62	1.73
PtRu/C@g-C3N4 NS	71.10	15.22	9.40	2.22	2.06

Table 2 Results of the fits of the Pt 4f spectra.

Catalysts	Species	Orbital spin	Binding energy/eV	Assignment	Relative content/ %
As-prepared PtRu/C	Pt 4f	$4f_{7/2}$	71.77	Pt	23.60
		$4f_{5/2}$	75.07	Pt	17.70
		$4f_{7/2}$	72.64	PtO	15.54
		$4f_{5/2}$	75.94	PtO	11.65
		$4f_{7/2}$	74.59	PtO_2	18.01
		$4f_{5/2}$	77.89	PtO_2	13.50
PtRu/C@ g-C_3N_4 NS	Pt 4f	$4f_{7/2}$	71.96	Pt	21.62
		$4f_{5/2}$	75.26	Pt	16.21
		$4f_{7/2}$	73.18	PtO	20.83
		$4f_{5/2}$	76.48	PtO	15.62
		$4f_{7/2}$	75.11	PtO_2	14.69
		$4f_{5/2}$	78.41	PtO_2	11.02

Table 3 Results of the fits of the Ru 3p spectra.

Catalysts	Species	Orbital spin	Binding energy/eV	Assignment	Relative content/ %
As-prepared PtRu/C	Ru 3p	$3p_{1/2}$	461.76	Ru	82.79
		$3p_{1/2}$	464.12	RuO_2	7.42
		$3p_{1/2}$	467.20	RuO_xH_y	9.79
PtRu/C@ g-C_3N_4 NS	Ru 3p	$3p_{1/2}$	462.58	Ru	48.40
		$3p_{1/2}$	465.11	RuO_2	40.65
		$3p_{1/2}$	468.84	RuO_xH_y	10.95

Fig. 5A shows the CV curves for the methanol electro-oxidation reaction (MOR) in an Ar-saturated solution of 0.5 mol L^{-1} H_2SO_4 containing 0.5 mol L^{-1} CH_3OH at a scanning rate of 50 mV s^{-1} at 25 °C. The forward peak current densities on the PtRu/C@g-C_3N_4 NS and PtRu/C catalysts are 1.14 and 0.54 A mg_{Pt}^{-1}, respectively, indicating that the catalytic activity of the PtRu/C@g-C_3N_4 NS greatly increased, which is a factor of 2.1 times higher than that of PtRu/C. In addition, that of the PtRu/C@bulk g-C_3N_4 sample is almost close to 0 A mg_{Pt}^{-1}, indicating the fact that bulk g-C_3N_4 cannot be used as PtRu support material due to its low electron conductivity. However, it has been effectively solved by exfoliating g-C_3N_4 shell of C@bulk g-C_3N_4 materials to layered g-C_3N_4 nanosheets, which coated carbon black uniformly.

For the anodic oxidation of methanol, the forward peak current density (I_f) is generally regarded as methanol oxidation on non-poisoned catalysts, while the backward peak current density (I_b) is associated with methanol oxidation on regenerated catalysts (after the removal of the carbonaceous intermediate).[50] Thus, a higher ratio indicates more effective removal of the poisoning species on

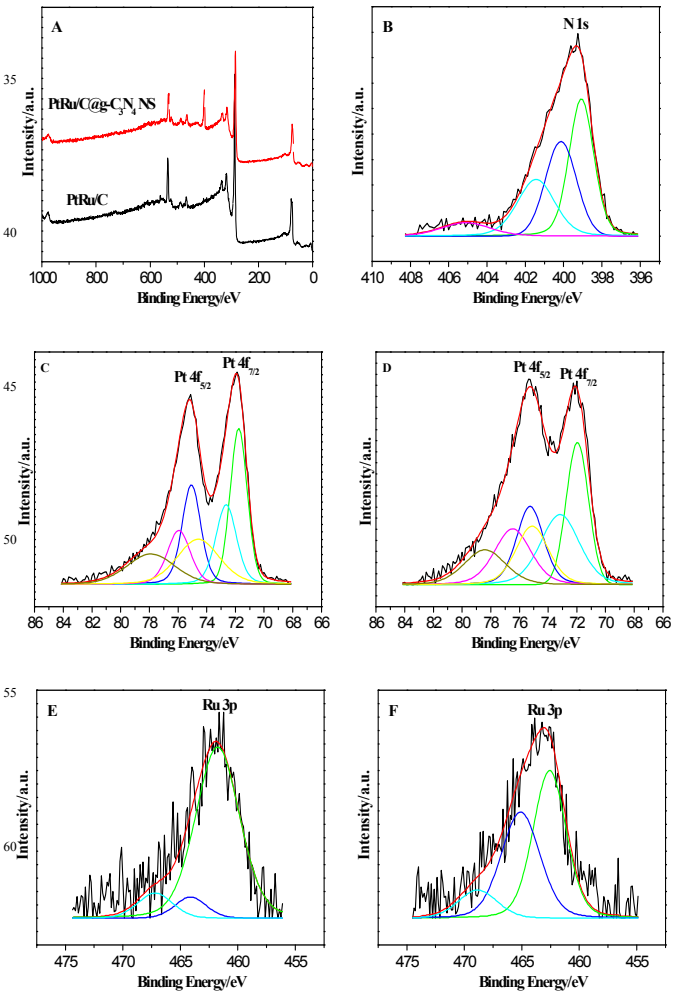

Fig. 4 XPS survey spectrum of PtRu/C and PtRu/C@g-C_3N_4 NS catalysts (A); XPS core level spectra of PtRu/C: (C) Pt 4f; (E) Ru 3p; XPS core level spectra of PtRu/C@g-C_3N_4 NS: (B) N 1s; (D) Pt 4f; (F) Ru 3p

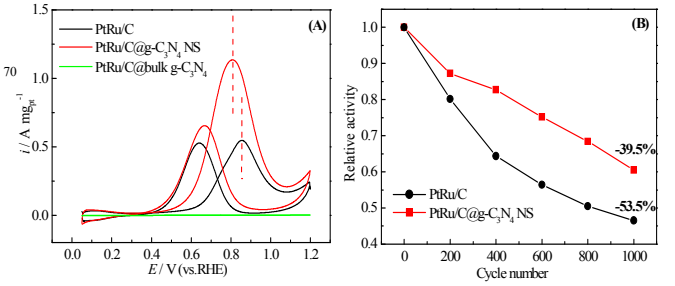

Fig. 5 A) Cyclic voltammograms of methanol electro-oxidation on the as-prepared PtRu/C, PtRu/C@g-C_3N_4 NS and PtRu/C@bulk g-C_3N_4 catalysts in an Ar-saturated solution of 0.5 mol L^{-1} CH_3OH and 0.5 mol L^{-1} H_2SO_4 at 25°C. Scanning rate: 0.05 V s^{-1}. B) The normalized peak current plots of methanol electro-oxidation for the PtRu/C@g-C_3N_4 NS and PtRu/C catalysts.

the catalyst surface. As calculated from Fig. 5A, the PtRu/C@g-C_3N_4 NS has a much higher I_f/I_b value (1.73) than PtRu/C (1.05), confirming that methanol molecules can be far more effectively oxidized to CO_2 on PtRu/C@g-C_3N_4 NS catalyst.

Fig. 6 shows the CO_{ad} stripping voltammograms for PtRu/C@g-C_3N_4 NS and as-prepared PtRu/C catalysts. The electrochemical

active surface area (ESA) is calculated with the recognised method based on the CO-stripping voltammetry curve.[51] The EAS of the PtRu/C and PtRu/C@g-C3N4 NS catalysts are about 73.4 and 96.8 $m^2 g^{-1}$. The increased electrochemical active surface area (ESA) or the remarkably high oxidation current for the PtRu/C@g-C_3N_4 NS compared to PtRu/C is directly related to the existence of g-C_3N_4, producing more sites for anchoring and deposition of Pt nanoparticles and reducing dissolution corrosion of support in acidic and oxidative environments. The specific activities of catalysts have also been given in Fig. S4 (in ESI for details†), which of the PtRu/C@g-C_3N_4 NS is 1.6 times higher than PtRu/C, comparing a lower factor of 2.1 times for the mass catalytic activity. This indicates the enhanced activity of PtRu/C@g-C_3N_4 NS partly due to the increase in the surface area in presence of oxides, as well as the stronger metal–support interaction between PtRu NPs and composite support. In addition, the onset potential for oxidation of adsorbed CO on PtRu/C@g-C_3N_4 NS catalyst shift to a lower electrode potential by 128.0 mV compared with the as-prepared PtRu/C. The negative potential shift should originate from the strong interaction between metal nanoparticles and nitrogen atoms and the changed electron structure of Pt is more appropriated for electrooxidation of adsorbed CO molecules on PtRu/C@g-C_3N_4 NS catalyst. This is consists with the fact that the PtRu/C@g-C_3N_4 NS catalyst has a much higher I_f/I_b ratio than as-prepared PtRu/C.

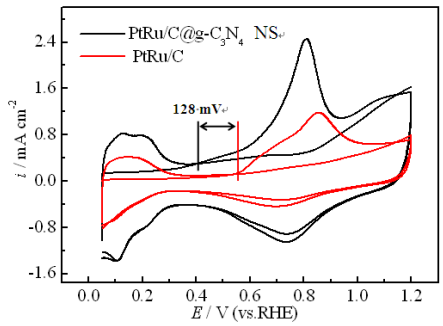

Fig. 6 The CO_{ad} stripping voltammetry on as-prepared PtRu/C and PtRu/C@g-C_3N_4 NS catalysts in a solution of 0.5 mol L^{-1} H_2SO_4 at 25°C. Scanning rate: 50 mV s^{-1}.

The long-time stability behavior of PtRu/C@g-C_3N_4 NS and PtRu/C catalysts toward methanol electro-oxidation are investigated by the continued CV cycles (see Fig. S3 in ESI for details†) as previously reported[34] and the normalized peak current densities are presented in Fig. 5B. It is particularly informative that PtRu/C has a sharp decline at 100 cycles and lost nearly 53.5% of its activity at 1000 cycles, compared with only 39.5% for PtRu/C@g-C_3N_4 NS. This result indicates that the latter behaves better catalytically and has stable properties for methanol oxidation, as is consistent with the CV above, chronoamperometric curves also result that PtRu/C@g-C_3N_4 NS catalyst has the excellent catalytic performance for methanol oxidation (see Fig. S5 in ESI for details†).

EIS was considered to investigate the properties of the new composite, including conductivity, structure, charge transfer and diffusion at the carbon–electrolyte interface. The Nyquist plots for PtRu/C@g-C_3N_4 NS and PtRu/C at 0.65 V potentials are shown in Fig. 7. It can be clearly seen that spectra exhibited strong contributions of inductive components at the high frequencies. This can be ascribed to the external circuit inductance and usually doesn't involve electrochemical process.[52] The large arc that appears at the medium frequency range relates to the electro-oxidation of methanol, and at the low frequency, this arc extends into the fourth quadrant and forms an induction loop that represents the electro-oxidation of $(CO)_{ad}$.[53, 54] An equivalent circuit representing the impedance behavior of the electrode was employed in this study and is shown in the inset of Fig. 7. According to the simulated parameters, the charge-transfer resistance (R_{ct}) in PtRu/C@g-C_3N_4 NS (30.7 Ω cm^2) is much lower than that of PtRu/C (53.6 Ω cm^2), which reveals that the rates of oxidation removal of the CO_{ad} by OH_{ad} are rapid on the PtRu/C@g-C_3N_4 NS catalyst.[55] In addition, comparing the fitting curves, the flattening measured spectrum is observed. The reason for this distortion is believed to be the roughness of the catalytic layer[56], or a current constriction effect[57].

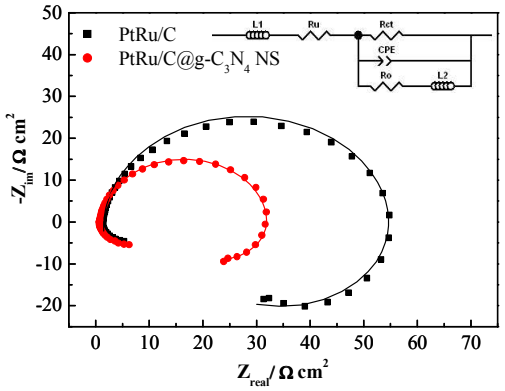

Fig. 7 Nyquist plots of EIS for PtRu/C and PtRu/C@g-C_3N_4 NS catalysts recorded in 0.5 M CH_3OH and 0.5 M H_2SO_4 at potential of 0.65 V; The inset is the equivalent circuit used for fitting the experimental data; the solid lines show fitted curves.

4. Conclusions

A novel approach to prepare graphitic carbon nitride nanosheets coated carbon black composite material for the first time has presented in this paper. It was characterized and tested as catalyst support materials for methanol electro-oxidation in an acidic medium. The results present the mass catalytic activity of the PtRu/C@g-C_3N_4 NS catalyst greatly increased, which is a factor of 2.1 times higher than that of PtRu/C catalyst. The excellent electrocatalytic ability and the unusually high poison tolerance due to the inherently excellent mechanical resistance and stability of g-C_3N_4 NS in acidic and oxidative environments, the increased electron conductivity of support by forming a core-shell structure of C@g-C_3N_4 NS, as well as the strong metal-support interaction between metal nanoparticles and composite support. Furthermore, the decrease of Pt(IV) composition in PtRu/C@g-C_3N_4 NS catalyst is also propitious to the improvement of the catalyst stability. Full testing of these supported catalysts in single cell fuel cells is in process. Based on this novel C@g-C_3N_4 NS hybrid nanostructure, many other interesting applications might also be discovered in areas such as heterogeneous catalysis, energy conversion and fuel cells, etc.

Acknowledgment

This research is financially supported by the National Natural Science Foundation of China (Grant No. 21273058), China postdoctoral science foundation (Grant No.2012M520731 and 2014T70350), Heilongjiang postdoctoral foundation (LBH-Z12089) and outstanding subject leaders of special fund project of Harbin in China (Grant No.2012RFXXG99).

References

1 R.T. Lv, T.X. Cui, M.S. Jun, Q. Zhang, A.Y. Cao, D.S. Su, Z.J. Zhang, S.H. Yoon, J. Miyawaki, I. Mochida, F.Y. Kang, *Adv. Funct. Mater.*, 2011, **21**, 999-1006.
2 S. Sharma, B.G. Pollet, *J. Power Sources*, 2012, **208**, 96-119.
3 Y.J. Wang, D.P. Wilkinson, J. Zhang, *Chem Rev*, 2011, **111**, 7625-7651.
4 X. Zhao, M. Yin, L. Ma, L. Liang, C. Liu, J. Liao, T. Lu, W. Xing, *Energy Environ. Sci.*, 2011, **4**, 2736-2753.
5 H.J. Cho, H. Jang, S. Lim, E. Cho, T.H. Lim, I.H. Oh, H.J. Kim, J.H. Jang, *Int. J. Hydrogen Energy*, 2011, **36**, 12465-12473.
6 A. Serov, C. Kwak, *Appl. Catal., B*, 2009, **90**, 313-320.
7 E.J. Biddinger, D.S. Knapke, D. von Deak, U.S. Ozkan, *Appl. Catal., B*, 2010, **96**, 72-82.
8 F.G. Welsch, K. Stowe, W.F. Maier, *ACS Comb. Sci.*, 2011, **13**, 518-529.
9 M.K. Debe, *Nature*, 2012, **486**, 43-51.
10 A. Walcarius, *Chem Soc Rev*, 2013, **42**, 4098-4140.
11 P. Joghee, S. Pylypenko, T. Olson, A. Dameron, A. Corpuz, H.N. Dinh, K. Wood, K. O'Neill, K. Hurst, G. Bender, T. Gennett, B. Pivovar, R. O'Hayre, *J. Electrochem. Soc.*, 2012, **159**, F768-F778.
12 K. Kakaei, M. Zhiani, *J. Power Sources*, 2013, **225**, 356-363.
13 H. Chhina, S. Campbell, O. Kesler, *J. Power Sources*, 2006, **161**, 893-900.
14 C. Alegre, M.E. Gálvez, E. Baquedano, R. Moliner, E. Pastor, M.J. Lázaro, *J. Phys. Chem. C*, 2013, **117**, 13045-13058.
15 K. Nam, S. Lim, S.K. Kim, S.H. Yoon, D.H. Jung, *Int. J. Hydrogen Energy*, 2012, **37**, 4619-4626.
16 J. Qi, L.H. Jiang, S.L. Wang, G.Q. Sun, *Appl. Catal., B*, 2011, **107**, 95-103.
17 L. La-Torre-Riveros, R. Guzman-Blas, A.E. Mendez-Torres, M. Prelas, D.A. Tryk, C.R. Cabrera, *ACS Appl. Mater. Interfaces*, 2012, **4**, 1134-1147.
18 C. Zhang, L. Xu, N. Shan, T. Sun, J. Chen, Y. Yan, *ACS Catal.*, 2014, **4**, 1926-1930.
19 D.P. He, C. Zeng, C. Xu, N.C. Cheng, H.G. Li, S.C. Mu, M. Pan, *Langmuir*, 2011, **27**, 5582-5588.
20 H. Huang, X. Wang, *J. Mater. Chem., A*, 2014, **2**, 6266.
21 J. Zhu, X. Zhao, M. Xiao, L. Liang, C. Liu, J. Liao, W. Xing, *Carbon*, 2014, **72**, 114-124.
22 B. Xiong, Y. Zhou, Y. Zhao, J. Wang, X. Chen, R. O'Hayre, Z. Shao, *Carbon*, 2013, **52**, 181-192.
23 X.F. Lu, H.J. Wang, S.Y. Zhang, D.L. Cui, Q.L. Wang, *Solid State Sciences*, 2009, **11**, 428-432.
24 Y. Zheng, J. Liu, J. Liang, M. Jaroniec, S.Z. Qiao, *Energy Environ. Sci.*, 2012, **5**, 6717-6731.
25 P. Niu, L. Zhang, G. Liu, H.-M. Cheng, *Adv. Funct. Mater.*, 2012, **22**, 4763-4770.
26 P. Xiao, Y. Zhao, T. Wang, Y. Zhan, H. Wang, J. Li, A. Thomas, J. Zhu, *Chemistry*, 2014, **20**, 2872-2878.
27 N. Mansor, A.B. Jorge, F. Cora, C. Gibbs, R. Jervis, P.F. McMillan, X. Wang, D.J. Brett, *J. Phys. Chem. C*, 2014, **118**, 6831-6838.
28 X.H. Li, M. Antonietti, *Chem Soc Rev*, 2013, **42**, 6593-6604.
29 J. Tian, R. Ning, Q. Liu, A.M. Asiri, A.O. Al-Youbi, X. Sun, *ACS Appl Mater Interfaces*, 2014, **6**, 1011-1017.
30 S. Yang, X. Feng, X. Wang, K. Müllen, *Angew. Chem. Int. Ed.*, 2011, **50**, 5339-5343.
31 A. Thomas, A. Fischer, F. Goettmann, M. Antonietti, J.-O. Müller, R. Schlögl, J.M. Carlsson, *J. Mater. Chem.*, 2008, **18**, 4893.
32 Q. Liu, J. Zhang, *Langmuir*, 2013, **29**, 3821-3828.
33 M. Kim, S. Hwang, J.S. Yu, *J. Mater. Chem.*, 2007, **17**, 1656-1659.
34 Z.-B. Wang, C.-Z. Li, D.-M. Gu, G.-P. Yin, *J. Power Sources*, 2013, **238**, 283-289.
35 Z.-Z. Jiang, Z.-B. Wang, Y.-Y. Chu, D.-M. Gu, G.-P. Yin, *Energy Environ. Sci.*, 2011, **4**, 2558-2566.
36 Y.Y. Chu, Z.B. Wang, Z.Z. Jiang, D.M. Gu, G.P. Yin, *Adv. Mater.*, 2011, **23**, 3100-3104.
37 H. Zhao, H. Yu, X. Quan, S. Chen, Y. Zhang, H. Zhao, H. Wang, *Appl. Catal., B*, 2014, **152-153**, 46-50.
38 D. Gao, Q. Xu, J. Zhang, Z. Yang, M. Si, Z. Yan, D. Xue, *Nanoscale*, 2014, **6**, 2577-2581.
39 Z.-B. Wang, X.-P. Wang, P.-J. Zuo, B.-Q. Yang, G.-P. Yin, X.-P. Feng, *J. Power Sources*, 2008, **181**, 93-100.
40 Y.Y. Chu, Z.B. Wang, Z.Z. Jiang, D.M. Gu, G.P. Yin, *Fuel Cells*, 2010, **10**, 914-919.
41 Y. Xu, X. Xie, J. Guo, S. Wang, Y. Wang, V.K. Mathur, *J. Power Sources*, 2006, **162**, 132-140.
42 J. Guo, G. Sun, S. Shiguo, Y. Shiyou, Y. Weiqian, Q. Jing, Y. Yushan, X. Qin, *J. Power Sources*, 2007, **168**, 299-306.
43 X. Zhang, H. Wang, H. Wang, Q. Zhang, J. Xie, Y. Tian, J. Wang, Y. Xie, *Adv. Mater.*, 2014, **26**, 4438-4443.
44 L. Ge, C. Han, *Appl. Catal., B*, 2012, **117-118**, 268-274.
45 H. Zhao, H. Yu, X. Quan, S. Chen, H. Zhao, H. Wang, *RSC Adv.*, 2014, **4**, 624.
46 X. Zhao, J. Zhu, L. Liang, C. Li, C. Liu, J. Liao, W. Xing, *Appl. Catal., B*, 2014, **154-155**, 177-182.
47 W. Li, A.M. Lane, *Electrochem. Commun.*, 2009, **11**, 1187-1190.
48 J.W. Long, K.E. Swider, C.I. Merzbacher, D.R. Rolison, *Langmuir*, 1999, **15**, 780-785.
49 D.R. Rolison, P.L. Hagans, K.E. Swider, J.W. Long, *Langmuir*, 1999, **15**, 774-779.
50 X.L. Yang, X.Z. Liu, X.Y. Meng, X.Y. Wang, G. Li, C.Y. Shu, L. Jiang, C.R. Wang, *J. Power Sources*, 2013, **240**, 536-543.
51 C.L. Green, A. Kucernak, *J. Phys. Chem. B*, 2002, **106**, 1036-1047.
52 Y.T. Wang, G.C. Liu, M. Wang, G.Y. Liu, J.L. Li, X.D. Wang, *Int. J. Hydrogen Energy*, 2013, **38**, 9000-9007.
53 I.-M. Hsing, X. Wang, Y.J. Leng, *J. Electrochem. Soc.*, 2002, **149**, A615-A621.
54 J.T. Muller, P.M. Urban, W.F. Holderich, *J. Power Sources*, 1999, **84**, 157-160.
55 D. He, K. Cheng, T. Peng, M. Pan, S. Mu, *J. Mater. Chem., A*, 2013, **1**, 2126.
56 A. Maritan, F. Toigo, *Electrochim. Acta*, 1990, **35**, 141-145.
57 J. Fleig, J. Maier, *J. Electrochem. Soc.*, 1997, **144**, L302-L305.

Graphics entry

Graphitic carbon nitride nanosheets coated carbon black as high-performance PtRu catalyst support material for methanol electrooxidation

Cun-Zhi Li,[ab] Zhen-Bo Wang,*[a] Xu-Lei Sui,[a] Li-Mei Zhang,[a] Da-Ming Gu[b] and Shuo Gu[c]

[a] School of Chemical Engineering and Technology, Harbin Institute of Technology, No.92 West-Da Zhi Street, Harbin, 150001 China

[b] School of Science, Harbin Institute of Technology, No.92 West-Da Zhi Street, Harbin, 150001 China

[c] Department of Electrical and Computer Engineering, The George Washington University, Washington, DC, 20052, USA

* Corresponding author. Tel.: +86-451-86417853; Fax: +86-451-86418616

E-mail address: wangzhb@hit.edu.cn

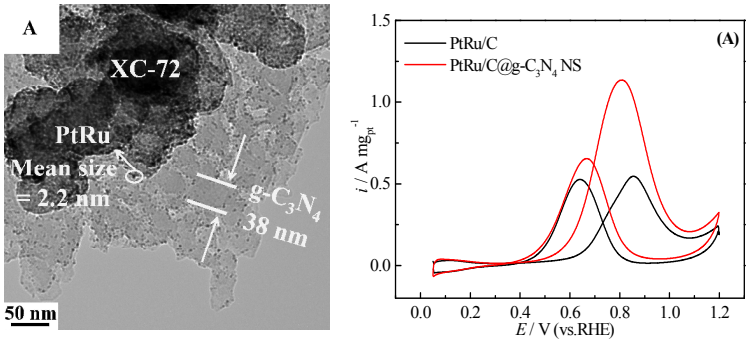

PtRu/C@g-C_3N_4 NS exhibits the excellent performance due to the inherently excellent mechanical resistance and stability of g-C_3N_4 NS and the strong metal-support interaction.